Molecular Therapy
Nucleic Acids
Original Article

In vivo production of engineered ACE2 decoy protects lungs from SARS-CoV-2 infection

Yuta Suzuki,[1] Takayuki Miyazaki,[1] Yoko Ida,[2] Tatsuya Suzuki,[3,4] Yumi Itoh,[3,4] Shuto Nakao,[3] Keita Kondo,[1] Kenji Kubara,[1] Keisuke Nishioka,[5] Hiroki Muto,[1] Ryuji Watari,[1] Toshifumi Hirayama,[2] Dai Kakiuchi,[1] Shinya Sato,[1] Satoshi Inoue,[1] Yoshifumi Uemoto,[1] Yohei Mukai,[2] Atsushi Hoshino,[6] Toru Okamoto,[3,4] and Junji Matsui[1]

[1]Tsukuba Research Laboratories, Eisai Co., Ltd., Ibaraki 300-2635, Japan; [2]Kobe Research Laboratories, Eisai Co., Ltd., Kobe 650-0047, Japan; [3]Department of Microbiology, Juntendo University School of Medicine, Tokyo 113-8421, Japan; [4]Research Institute for Microbial Diseases, Osaka University, Osaka 565-0871, Japan; [5]Department of Infectious Diseases, Graduate School of Medical Science, Kyoto Prefectural University of Medicine, Kyoto 602-8566, Japan; [6]Department of Cardiovascular Medicine, Graduate School of Medical Science, Kyoto Prefectural University of Medicine, Kyoto 602-8566, Japan

Severe acute respiratory syndrome coronavirus-2 (SARS-CoV-2) variants repeatedly evade the immune system within short periods. Thus, next-generation therapeutics that are resistant to mutations and can be rapidly supplied to individuals in an emergency are required. Here, we designed an mRNA encoding an engineered angiotensin-converting enzyme 2 (ACE2) decoy, 3N39v4, composed of high-affinity ACE2 and a human immunoglobulin G Fc domain. The 3N39v4-encoded mRNA was encapsulated in lipid nanoparticles for efficient *in vivo* delivery. Systemic delivery of mRNA in mice resulted in a dose-dependent expression of 3N39v4 in plasma (20–261 μg/mL at 1–10 mg/kg) with sufficient tolerability. An improved pharmacokinetic profile of the produced protein was compared to injection of the 3N39v4 protein. *In vivo*-expressed 3N39v4 exhibited broad neutralization against nine SARS-CoV-2 variants and other sarbecoviruses, including the currently circulating Omicron subvariants JN.1 and BA.2.86. A single intravenous injection of 3N39v4-encoded mRNA resulted in a robust, dose-dependent improvement in the outcomes of mice infected with SARS-CoV-2. The mRNA treatment in monkeys produced 3N39v4 in sera, which inhibited the replication of the authentic viruses. The rapid development of mRNA drugs highlights the potential of mRNA-encoded ACE2 decoys in emergencies to combat diverse SARS-CoV-2 variants, including future variants.

INTRODUCTION

The COVID-19 pandemic highlighted the importance of preventive and therapeutic drugs.[1] Ensuring a rapid global supply of these drugs on a large scale is crucial.[2] mRNA vaccines were quickly developed and successfully distributed worldwide.[3] This achievement was facilitated in part by the properties of chemically synthesized mRNA, which bypassed the complexities associated with the manufacturing of biologics.[4] However, although multiple monoclonal antibodies (mAbs) and antiviral drugs have been approved for emergencies, there is room for improvement in their supply rate.[5,6] Therefore, it is highly desirable to develop new and effective therapeutic strategies that can be developed rapidly.

The mRNA-based therapeutic scope has broadened beyond the success of mRNA vaccines.[7,8] These therapeutics utilize mRNA to produce proteins within the body, including intracellular enzymes, cytokines, and mAbs.[9,10] Currently, various mRNA encoding mAbs have been applied to infectious diseases (human immunodeficiency virus-1,[11,12] hepatitis B virus,[13] chikungunya virus,[14] SARS-CoV-2,[15,16] *Salmonella/Pseudomonas aeruginosa*,[17] and oncologic diseases [anti-CD3/anti-CLDN6 bispecific,[18] anti-CCL2/CCL5 bispecific,[19] anti-HER2,[20] anti-PD-1,[21] and anti-Claudin 18.2[22]]). The first report of mRNA-encoded proteins (i.e., mAb against chikungunya virus) showed *in vivo* expression in a phase 1 clinical trial.[23] This successful validation in humans highlights the potential of mRNA-encoded proteins as alternatives to conventional proteins.

To date, several mAbs targeting the SARS-CoV-2 spike protein have been granted Emergency Use Authorization in the United States.[24] However, the limitless emergence of SARS-CoV-2 variants evades neutralization of approved mAbs.[24] To overcome the critical issue of immune escape, we previously developed an engineered angiotensin-converting enzyme 2 (ACE2) by optimizing amino acids to enhance its affinity by ∼100-fold for the SARS-CoV-2 spike protein, which resulted in a neutralization activity comparable to that of mAbs.[25] The engineered ACE2 decoy (3N39v4) is expected to resist viral immune escape because mutated viruses that evade the ACE2 decoy do not bind to endogenous ACE2 receptors on host cells, thereby diminishing their infectivity.[26]

Received 15 October 2024; accepted 24 January 2025;
https://doi.org/10.1016/j.omtn.2025.102467.

Correspondence: Yuta Suzuki, Tsukuba Research Laboratories, Eisai Co., Ltd., Ibaraki 300-2635, Japan.
E-mail: y14-suzuki@hhc.eisai.co.jp
Correspondence: Atsushi Hoshino, Department of Cardiovascular Medicine, Graduate School of Medical Science, Kyoto Prefectural University of Medicine, Kyoto 602-8566, Japan.
E-mail: a-hoshi@koto.kpu-m.ac.jp
Correspondence: Toru Okamoto, Department of Microbiology, Juntendo University School of Medicine, Tokyo 113-8421, Japan.
E-mail: toruokamoto@juntendo.ac.jp

Published by Elsevier Inc. on behalf of The American Society of Gene and Cell Therapy.
This is an open access article under the CC BY-NC-ND license (http://creativecommons.org/licenses/by-nc-nd/4.0/).

Here, we combined two platforms: mRNA technology with the advantage of rapid supply and an engineered ACE2 decoy exhibiting resistance to virus mutations. We recently reported the development of a lipid nanoparticle (LNP)[27–29] that effectively delivered mRNA to the liver.[30] In this study, we developed mRNA encoding an engineered ACE2 decoy (3N39v4) and demonstrated its potential as a next-generation therapeutic.

RESULTS

Design of mRNA encoding an engineered ACE2 decoy (3N39v4)

We designed mRNA encoding an engineered ACE2 decoy. The engineered ACE2 receptor fused with human immunoglobulin G1 (IgG1) Fc, 3N39v4,[31] was encoded into chemically modified mRNA bearing 5'Cap1, 5' UTR, 3' UTR, and poly(A) tail with 100 nt (Figure 1A). To suppress unwanted immune reaction and increase protein production, all uridine was fully replaced with N1-methylpseudouridine (N1mΨ) as previously reported.[32,33] The prepared 3N39v4 mRNA was formulated into an LNP formulation based on the ionizable lipid L202 that was recently reported for mRNA delivery.[34,35] The representative LNP-formulated 3N39v4 mRNA had a size of 68 nm, a polydispersity index of 0.08, and 98% mRNA encapsulation; the morphology of homogeneous particles was revealed using cryoelectron microscopy (cryo-EM) (Figures S1A and S1B). The pKa value of LNP-mRNA by the 6-(p-toluidino)-2-naphthalenesulfonic acid sodium salt (TNS) fluorescent assay was 6.58 and the zeta potential was −0.164 mV (Figure S1C). LNP-formulated mRNA is mainly delivered to the liver following intravenous injection.[36] Therefore, with an aim toward human applications, primary human hepatocytes were treated with 3N39v4 mRNA and luciferase mRNA in LNPs. After 48 h, the supernatant was evaluated using two types of ELISA that detect binding with either the Fc region of human IgG or the receptor-binding domain (RBD) of the SARS-CoV-2 spike (Figure 1B). Treatment with LNP-3N39v4 mRNA increased protein concentration in a dose-dependent manner for both quantification methods (Figure 1B). Importantly, the secreted 3N39v4 in the supernatant showed the same binding affinity to the RBD as recombinant 3N39v4 in protein form, demonstrating that mRNA-expressed 3N39v4 has functional binding activity (Figure 1C). The 3N39v4 mRNA encodes a monomeric fragment (970 amino acids, ∼111.4 kDa), which in turn forms a disulfide-bonded homodimer-like IgG to produce 3N39v4 (∼222.7 kDa). To determine whether 3N39v4 was properly expressed in cells following LNP mRNA treatment, we performed SDS-PAGE analysis using recombinant 3N39v4 as a reference (Figure 1D). The 3N39v4 from Expi293F cells formed disulfide-bonded homodimers under oxidative conditions (without dithiothreitol, DTT(−)), and the molecular weight of the monomeric fragment fit the theoretical value under reduced conditions [with dithiothreitol, DTT(+)] (Figure 1D). Cryo-EM analysis revealed that 3N39v4 was expressed in an IgG-like form that supports the homodimer formation (Figure 1E). Furthermore, the binding of 3N39v4 to the SARS-CoV-2 spike protein was investigated using size-exclusion chromatography (SEC; Figure S2). The expressed 3N39v4 co-eluted with recombinant SARS-CoV-2 spike trimers, with the elution peaks of the complex shifting to larger molecular sizes than those of recombinant 3N39v4 and the spike protein (Figure S2). This indicates that 3N39v4 functionally bound to the spike and formed a complex. Overall, the designed 3N39v4 mRNA produced functional 3N39v4 in human hepatocytes, with characteristics similar to those of recombinant 3N39v4.

Pharmacokinetic profile of 3N39v4 mRNA in mice

To characterize the plasma concentration-time profile, CD-1 mice (n = 5) received a single administration of 1 mg/kg LNP-formulated 3N39v4 mRNA and 5 mg/kg recombinant 3N39v4 in protein format (Figure 2A). The 3N39v4 mRNA showed robust and durable plasma concentrations compared to that of recombinant 3N39v4 (Figure 2B). The recombinant 3N39v4 plasma concentration was highest (39.0 μg/mL [C_{max}]) at 0.5 h after injection, then decreased and became undetectable by day 7 (Figure 2C). In contrast, the 3N39v4 plasma levels by treatment of 3N39v4 mRNA increased after administration, reaching a peak concentration of 26.7 μg/mL (C_{max}) at 43.2 h, and exhibited durable expression for 10 days (Figure 2C). Importantly, the area under the curve of 3N39v4 mRNA was significantly (4.3-fold) higher than that of recombinant 3N39v4 (i.e., 3,930 for mRNA vs. 922 for protein, h * μg/mL; $p < 0.05$) (Figure 2C). Furthermore, the remaining 3N39v4 mRNA in the liver was measured using qPCR (Figure S3). The time-concentration profile showed that the mRNA was eliminated over 10 days, supporting the sustained expression of 3N39v4 in the systemic circulation (Figure S3). To determine whether 3N39v4 in the mouse plasma functionally binds to the RBD, we tested its binding affinity using 3N39v4-containing pooled mouse plasma (Figure 2D). The binding-affinity profile of 3N39v4 in mouse plasma was identical to that of recombinant 3N39v4, demonstrating the unimpaired binding activity of *in vivo*-produced 3N39v4 (Figure 2D). Overall, a single administration of LNP-formulated 3N39v4 mRNA showed improved plasma pharmacokinetics compared to those of recombinant 3N39v4.

Dose-dependent activity and tolerability of 3N39v4 mRNA in mice

We further validated the 3N39v4 mRNA *in vivo*. To confirm this dose-dependent activity, CD-1 mice received saline or LNP-formulated 3N39v4 at 1, 3, or 10 mg/kg mRNA (Figure 2E). The concentration of 3N39v4 in mouse plasma increased in a dose-dependent manner, reaching a maximum of 261.2 μg/mL at 3 days post-administration of 10 mg/kg mRNA (Figure 2F). Next, we evaluated the neutralization activity (NT_{50} titer) of endogenously expressed 3N39v4 using a SARS-CoV-2 pseudovirus (D614G strain) and serially diluted mouse plasma (Figure 2G). Robust neutralization was observed in a dose-dependent manner (NT_{50} titer: 567-fold, 1,813-fold, 5,640-fold dilution at 1, 3, and 10 mg/kg, respectively) (Figure 2G). The calculated half-maximal inhibitory concentration (IC_{50}) (i.e., 3N39v4 concentration at day 3 divided by NT_{50} titer) was 0.035, 0.028, and 0.046 μg/mL for 1, 3, and 10 mg/kg doses, respectively, which was similar to the previously reported IC_{50} value (0.0389 μg/mL) of 3N39v4 in protein format using the same pseudovirus (D614G) neutralization assay.[26] Finally, we evaluated the tolerability of a single dose of 3N39v4 mRNA in mice. Body weight changes in the mRNA-treated group at all doses were

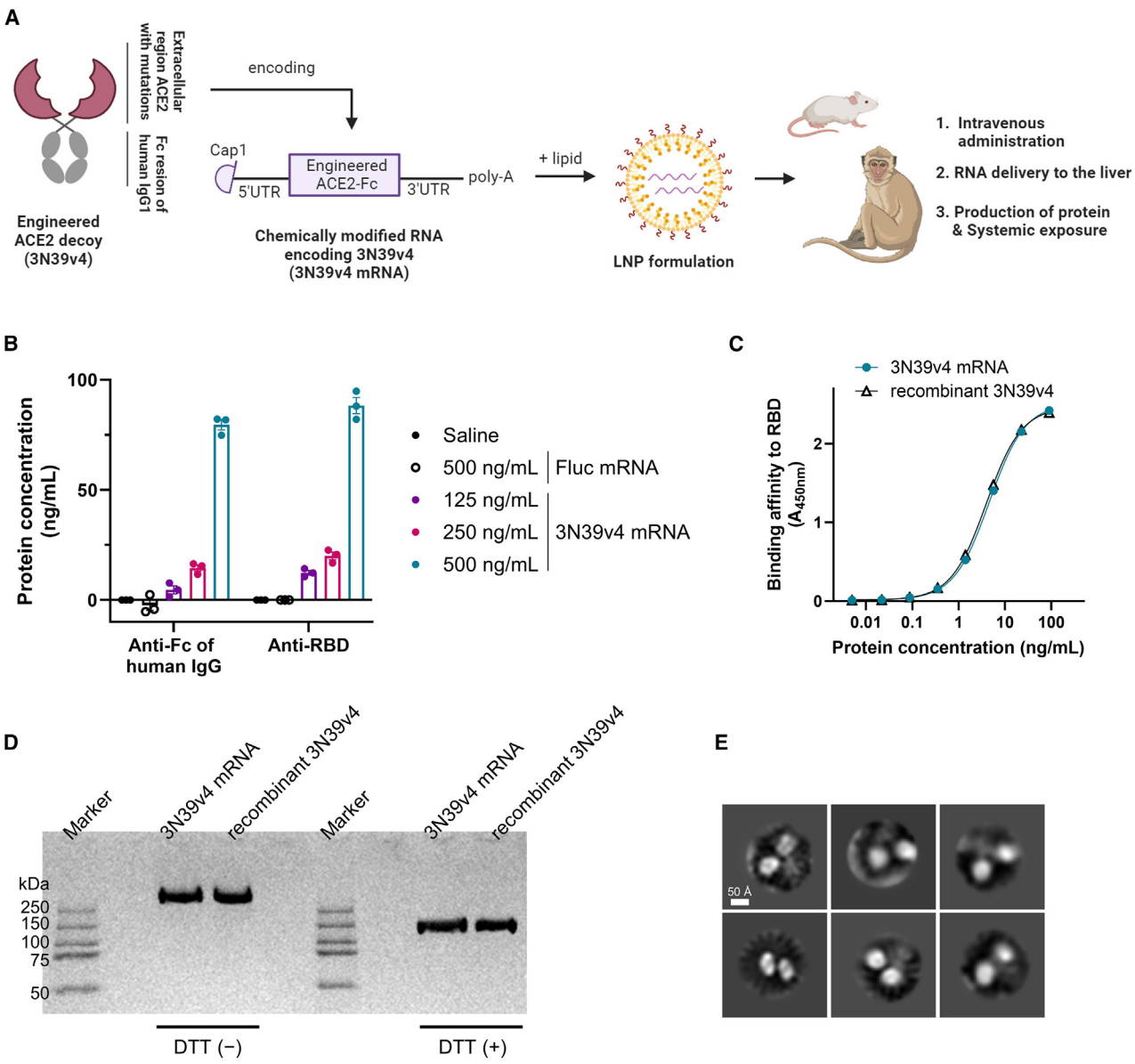

Figure 1. Design of mRNA encoding an engineered ACE2 decoy

(A) mRNA-based therapy against SARS-CoV-2 infection. Engineered ACE2 receptor fused with human IgG1 Fc (3N39v4) was encoded into chemically modified mRNA with N1mΨ (3N39v4 mRNA). 3N39v4 mRNA was formulated into lipid nanoparticles (LNPs) and intravenously administrated *in vivo*. (B) We treated 3N39v4 expression in primary human hepatocytes with LNP-3N39v4 mRNA; 3N39v4 concentration in supernatant was measured by two types of ELISA, detecting the Fc region of human IgG or the receptor-binding domain (RBD) of SARS-CoV-2 spike protein. Data are shown as means ± SEMs. (C) Binding affinity to the RBD of either recombinant 3N39v4 as reference or 3N39v4 in supernatant from primary human hepatocytes treated with LNP-3N39v4 mRNA. Data are presented as the mean of $n = 2$ technical replicates. (D) The SDS-PAGE profile of either recombinant 3N39v4 or 3N39v4 from cells treated with LNP-3N39v4 mRNA. The proteins were analyzed with the original and reduced states using dithiothreitol (DTT). (E) Two-dimensional class averaged cryoelectron microscopy (cryo-EM) images of 3N39v4 from cells treated with LNP-3N39v4 mRNA.

similar to those in the saline-treated group (Figure 2H). Aspartate transaminase (AST) and alanine aminotransferase (ALT) levels increased slightly at a dose of 10 mg/kg on day 1 and returned to the same levels as those in the saline-treated group on day 3 (Figures S4A and S4B). There were no apparent changes in the other clinical chemistry parameters (Figure S4C). These data demonstrate that a single dose of LNP-formulated 3N39v4 was well tolerated at a dose of 1–10 mg/kg. Collectively, 3N39v4 mRNA delivery produced a neutralizing ACE2 decoy in mice with a feasible safety profile.

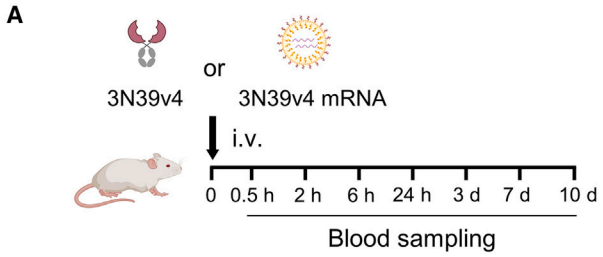

C

	Recombinant 3N39v4 (5 mg/kg, n=5)	3N39v4 mRNA (1 mg/kg, n=5)
C_{max} (μg/mL)	39.0	26.7
T_{max} (h)	0.5	43.2
AUC_{0-t} (h*μg/mL)	922	3930

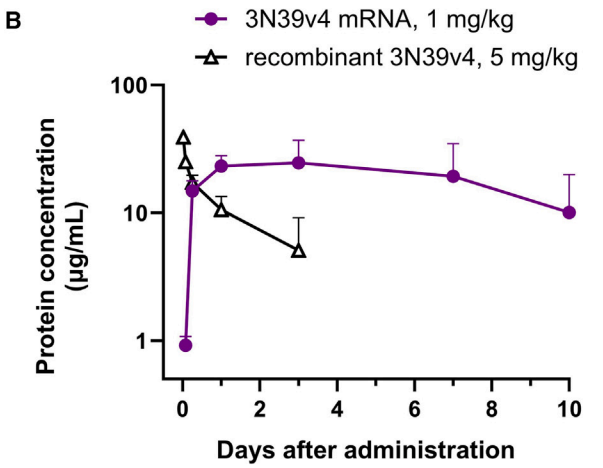

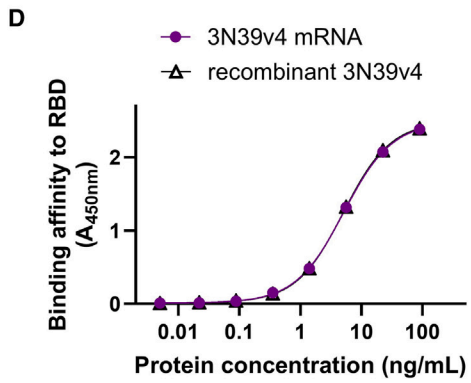

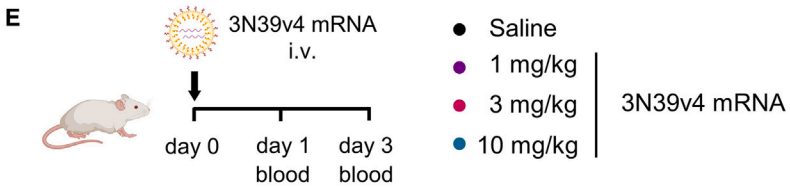

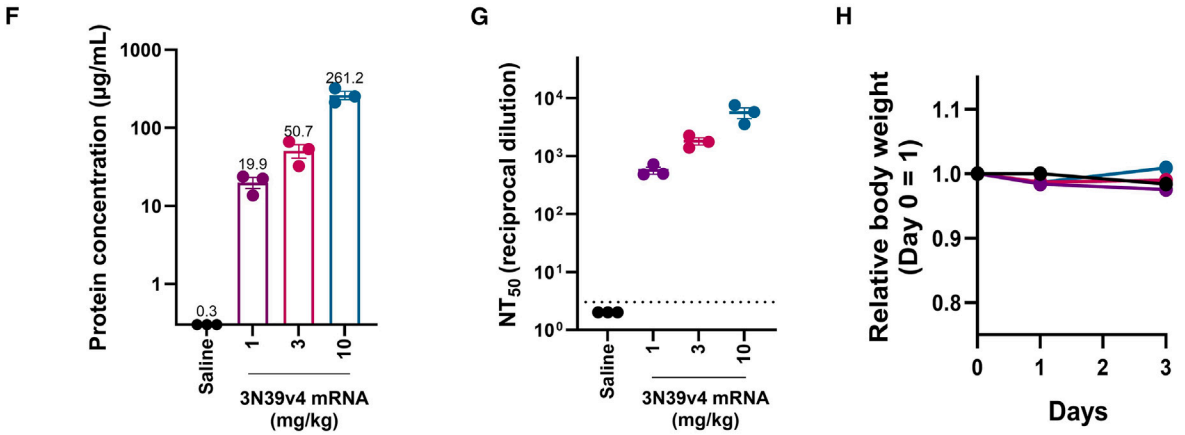

Figure 2. *In vivo* validation of 3N39v4 mRNA

(A–D) Pharmacokinetics profile in mice. (A) Experimental design. Male CD-1 mice ($n = 5$) received a single intravenous administration of either recombinant 3N39v4 in protein format at 5 mg/kg or LNP-3N39v4 mRNA at 1 mg/kg. At the indicated time points, 3N39v4 concentration in mice plasma was measured by ELISA. The lower limit of quantification is 0.01 μg/mL. Data are shown as means ± SDs. (B) Pharmacokinetics analysis. (C) The binding affinity to the RBD of 3N39v4 in mouse plasma (pooled, $n = 5$/group) treated with either (D) recombinant 3N39v4 or 3N39v4 mRNA. (E–H) Dose-dependent activity and tolerability in mice. (E) Experimental design. Male CD-1 mice

(legend continued on next page)

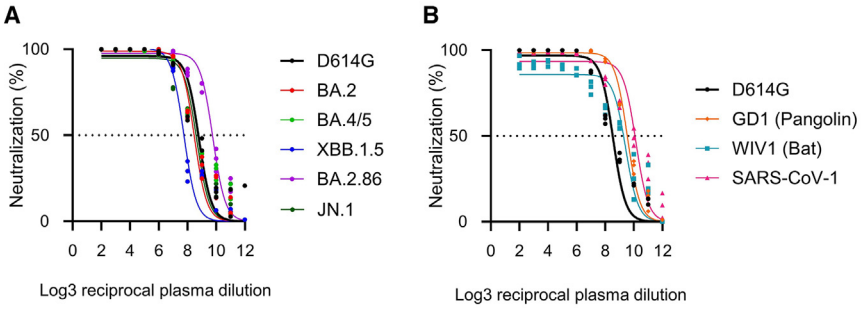

Figure 3. Broad neutralization activity of *in vivo* produced 3N39v4

CD-1 mouse plasma samples 3 days after a 10-mg/kg dose of LNP-3N39v4 mRNA were pooled (n = 3) and used as 3-fold serial dilution. Neutralization of (A) SARS-CoV-2 variants and (B) SARS-related coronaviruses against the pseudovirus. The data are presented as n = 3 technical replicates.

In vivo 3N39v4 broadly neutralizes Omicron subvariants and sarbecoviruses

We examined the breadth of cross-neuralization using nine pseudoviruses (Figure 3). The pooled mouse plasma on day 3 after administration of 10 mg/kg 3N39v4 mRNA was used as a 3-fold serial dilution. Endogenously produced 3N39v4 in mice showed broad neutralization efficacy against D614G and all the Omicron subvariants tested (Figure 3A). Importantly, it neutralized the currently circulating Omicron subvariants JN.1 and BA.2.86, as well as the recent XBB.1.5, which evaded bebtelovimab, the only mAb effective against both BA.2 and BA.4/5 in clinical use (Figure 3A).[37] In addition, it robustly neutralized other sarbecoviruses, including GD1, WIV1, and SARS-CoV-1 (Figure 3B). Overall, *in vivo* expression of 3N39v4 broadly neutralized the currently circulating Omicron subvariant and other sarbecoviruses.

Prophylactic and therapeutic efficacy of 3N39v4 mRNA in mice

We investigated the protective efficacy of 3N39v4 mRNA in a well-established infectious mouse model using a mouse-adapted SARS-CoV-2 MA10 strain.[38] A single-dose, dose-dependent study was conducted under prophylactic conditions (Figure 4A). Based on the pharmacokinetic, dose-dependent, and tolerability studies in mice, we selected the 24-h pre-dose and the 1- to 3-mg/kg mRNA dose. Mice were treated with saline or 3N39v4 mRNA on day 0. All animals were intranasally infected with MA10 on day 1. On the day of necropsy (day 5), mRNA treatment significantly reduced viral RNA (p = 0.0958 for 1 mg/kg, p = 0.0001 for 3 mg/kg) and viral titers (p = 0.0001 for 1 mg/kg, p < 0.0001 for 3 mg/kg) in the lungs, in a dose-dependent manner (Figure 4B). The expression of genes encoding inflammatory cytokines, such as interleukin-6 (*IL-6*), C-X-C motif chemokine 10 (*CXCL10*), and chemokine ligand 3 (*CCL3*), but not *CCL5*, was significantly attenuated in the treated mice (Figure 4C). Histopathological examination of randomly selected lung tissues showed severe lung inflammation characterized by extensive infiltration of inflammatory cells and alveolar hemorrhage in control mice. Importantly, these pathological changes were significantly alleviated in treated mice (Figures 4D and 4E). Moreover, immunohistochemical staining of the SARS-CoV-2 nucleocapsid in selected lung tissues revealed that the presence of nucleocapsids observed in control mice was almost completely undetectable in the treated mice (Figures 4F and 4G).

Encouraged by its robust activity under prophylactic conditions, we conducted a single-dose, dose-dependent study under therapeutic conditions (Figure 5A). Mice were intranasally inoculated with MA10 on day 0. After 3 h of infection, the mice were treated with saline or 3N39v4 mRNA and sacrificed on day 4. Importantly, 3N39v4 mRNA treatment significantly inhibited viral RNA and viral titers in a dose-dependent manner (Figure 5B). Gene expression of inflammatory cytokines, histopathological examination, and immunohistochemical staining of the lungs demonstrated robust protection against SARS-CoV-2 (Figures 5C–5G). Collectively, 3N39v4 mRNA conferred robust protective efficacy in the SARS-CoV-2 MA10 model under both prophylactic and therapeutic conditions.

Biodistribution of LNP in monkeys

Non-human primates are generally considered the most predictive model of human responses.[39] To estimate the biodistribution of our L202-based LNP in humans, we used luciferase-encoded mRNA and cynomolgus monkeys. Cynomolgus monkeys were administered LNP-formulated luciferase mRNA, and tissues were collected after 24 h to measure relative luciferase luminescence (luminescence per unit of protein tissue weight) (Figure 6A). The 24-h post-dose time point was selected since the majority of LNPs are expected to have been distributed to the organs, based on the previous report of the pharmacokinetic profile of LNP-mRNA in non-human primates.[39] The highest luminescence was observed in the liver (Figure 6B). Signals were detected in the spleen and the mandibular lymph nodes. Negligible signals were observed in other tissues, including the kidneys, lungs, heart, pancreas, bone marrow, and mesenteric lymph nodes (Figure 6B). These data show that our L202-based LNP-mRNA predominantly targeted the liver in monkeys.

(n = 3) received a single intravenous dose of either saline or LNP-3N39v4 mRNA (1, 3, or 10 mg/kg mRNA). (F and G) The 3N39v4 concentration in (F) mouse plasma and (G) NT_{50} titer on day 3. (H) Body weight change. NT_{50} titer was evaluated by SARS-CoV-2 pseudovirus (D614G strain) neutralization assay using 3-fold serial dilution of plasma. Data are shown as means ± SEMs (F–H). Dot line is limit of detection. AUC_{0-t}, area under the curve; C_{max}, maximum plasma concentration; T_{max}, time-to-maximum blood concentration; NT_{50}, 50% neutralizing titer.

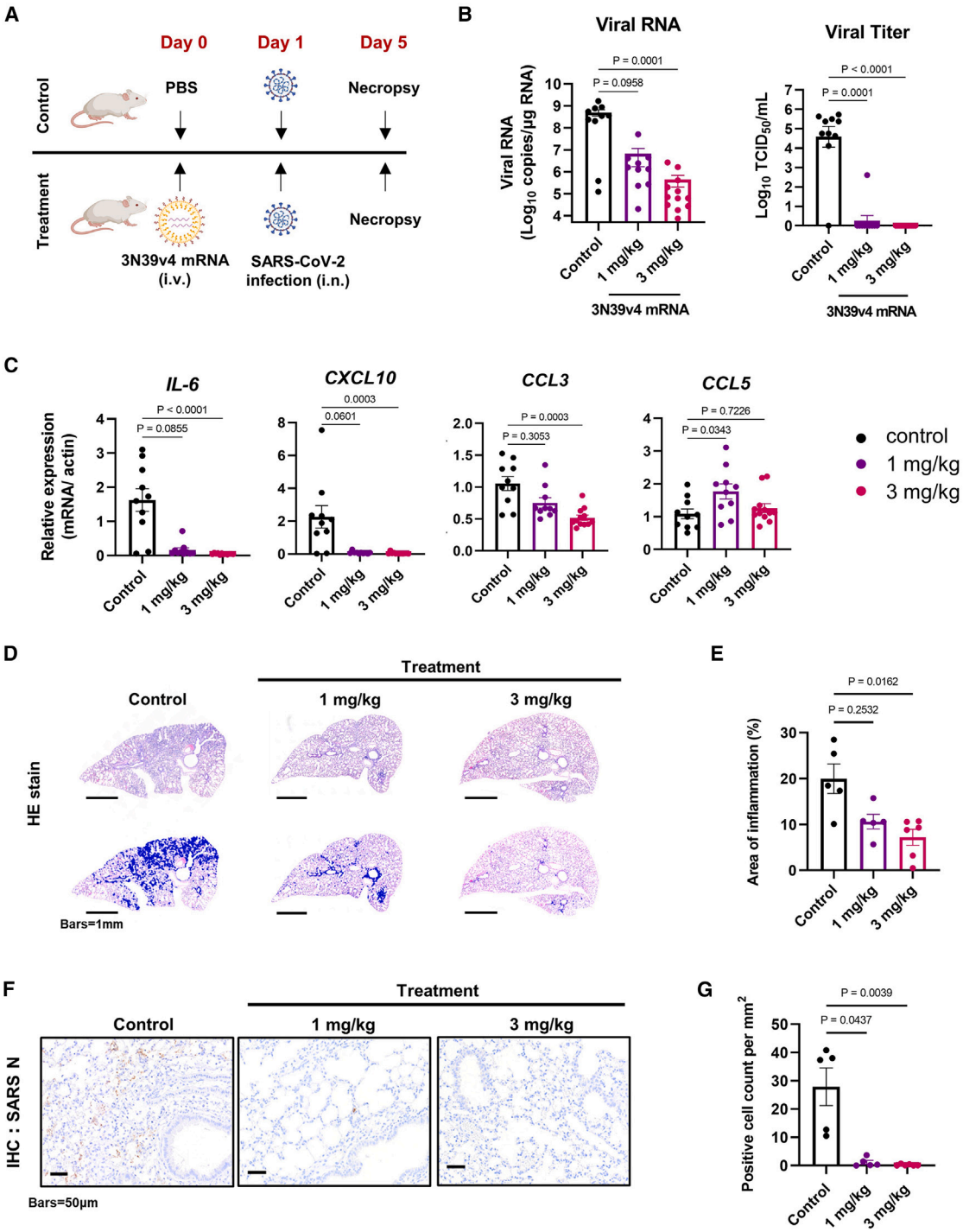

Figure 4. Prophylactic efficacy of 3N39v4 mRNA

(A) Experimental design. BALB/c mice were pretreated with a single intravenous administration of either PBS (n = 10), 3N39v4 mRNA at 1 mg/kg (n = 10), or 3 mg/kg (n = 12) at day 0. Then, mice were intranasally (i.n.) inoculated with MA10 at 1.0×10^4 $TCID_{50}$ (in 20 μL) at day 1 and sacrificed at day 5. (B) Viral replication was measured in the lung. At the time of euthanasia, lung tissues were minced to measure viral RNA abundance (left) and viral titer (right) by qPCR analysis and $TCID_{50}$. (C) mRNA expression of IL-6, CXCL10, CCL3, and CCL5 in the lungs are shown for the control and treatment groups at day 5. (D) Hematoxylin and eosin (H&E) staining for lung tissue sections of mice in

(legend continued on next page)

3N39v4 mRNA produced a functional ACE2 decoy in monkeys

To assess its potential applicability in humans, the 3N39v4 mRNA levels were evaluated in non-human primates. Cynomolgus monkeys received LNP-formulated 3N39v4 mRNA at 1 mg/kg (Figure 7A). Two monkeys showed a rapid increase in 3N39v4 serum levels on day 1, which were maintained through day 7 and were detectable until day 14 (Figure 7B). The C_{max} reached 5.5 μg/mL at 48 h post-administration. PCR quantification demonstrated the elimination of 3N39v4 mRNA from the serum over 7 days (Figure 7C). With high concentrations persisting from day 1 (4.7 μg/mL) to day 7 (4.4 μg/mL), serum samples from days 1, 4, and 7 underwent functional assays. All sera from days 1–7 substantially neutralized the SARS-CoV-2 pseudovirus (D614G strain) (Figure 7D). The calculated IC_{50} in monkey sera was 0.057 μM (day 1), 0.023 μM (day 4), and 0.021 μM (day 7), which were comparable to those observed in mice. Next, we evaluated the neutralization activity using authentic SARS-CoV-2 Omicron subvariants XBB.1 and BA.2.75 (Figure 7E). Owing to the limited number of samples, individual monkey sera from days 1, 4, and 7 were pooled to complete the assay. Importantly, two pooled monkey sera (final 2-fold dilution) completely inhibited the replication of XBB.1 and BA.2.75 (Figure 7E). Furthermore, 3N39v4 mRNA administration did not have a significant influence on clinical signs, body weight, or serum AST/ALT levels in the two monkeys (Figures S5A–S5C). The level of pro-inflammatory cytokine IL-6 was transiently elevated following administration and returned to that at the baseline after 24 h (Figure S5D). Other potential risks in the development of protein-based formulations include immunogenicity[40] and off-target binding against endogenous components.[41] In T cell assays using 50 different HLA donors, recombinant 3N39v4 showed similar or lower immunogenicity than the benchmark antibody herceptin, used in the clinic (Table S1). In off-target binding assays, recombinant 3N39v4 showed negligible binding activity with representative biological components, including carbohydrates, single-stranded DNA, double-stranded DNA, and bovine serum albumin (Figure S6). These data demonstrated that 3N39v4 has low immunogenicity and polyreactivity. Overall, 3N39v4 mRNA produced 3N39v4 in non-human primates with a sufficient safety profile and neutralized authentic Omicron subvariants.

DISCUSSION

Although the mRNA-encoding antibody against SARS-CoV-2 has been described previously,[15,16] a critical issue is the immune escape of the virus.[24,37] The emergence of subvariants, such as XBB, completely evaded the authorized antibodies casirivimab/imdevimab (Ronapreve), tixagevimab/cilgavimab (Evusheld), and bebtelovimab.[24] We report for the first time, mRNA encoding an engineered ACE2 decoy, 3N39v4. The mRNA delivery by LNP formulation produced functionally active 3N39v4 *in vitro* and *in vivo*. The *in vivo* 3N39v4 was confirmed to broadly neutralize representative SARS-CoV-2 variants, including the currently circulating Omicron subvariants JN.1 and BA.2.86, demonstrating that 3N39v4 overcame immune escape.

The use of mRNA-encoded proteins/antibodies offers several advantages over conventional protein/antibody approaches. One of its primary advantages is rapid medical supply, which is crucial during outbreaks of emerging infections. In some cases, protein-based formulations present challenges for rapid supply owing to the complexity of manufacturing.[42] In contrast, the track record of the mRNA vaccine mRNA-1273 demonstrated that the initial clinical trial started only 66 days after the release of coronavirus sequences.[3] The unprecedented speed is due to strengths in the mRNA-based formulation. First, mRNA and LNP formulations are chemically (or enzymatically) manufactured without biological processes, such as cell culture in a bioreactor.[2] A long time (∼6 months) is required to establish a master cell bank to ensure uniform protein and antibody production from batch to batch.[5] The mRNA-based formulation can shorten the development time by circumventing the time required for biologics. Second, various mRNAs with different sequences or lengths can be formulated with LNP using a similar formulation process, and the resulting LNP-mRNAs exhibit similar physicochemical properties.[43] In the case of protein formulation, considerable effort is sometimes required to optimize manufacturing conditions and formulation design.[42] The commonality of the physicochemical properties of LNP-mRNAs allows for a shorter development time.

Another advantage of mRNA-encoded proteins is their improved *in vivo* pharmacokinetic profile. Most protein formulations are eliminated from the body quickly.[44,45] Various techniques have been effectively employed to prolong the half-life of approved protein-based drugs, including fusion to biomolecules, such as albumin and Fc regions, and attachment to synthetic polymers such as polyethylene glycol.[44,45] The 3N39v4 protein in mice was detectable after 3 days of administration owing to FcRn receptor-mediated recycling by the fused Fc region. Importantly, *in vivo* production of 3N39v4 by mRNA treatment further extended its half-life, with durable expression observed for 10 days after administration. This improvement likely stems from the continuous liver-derived mRNA-encoded 3N39v4 protein supply to systemic circulation.[23] This mRNA-based formulation offers an alternative approach to extend the half-life of biologics, which is particularly advantageous for protein-based drugs. mRNA-based formulations have the potential to provide infectious disease protection with a single dose.

The 3N39v4 mRNA demonstrated clear dose-dependent efficacy in infected mice. The suppression of pulmonary inflammation suggests that 3N39v4 effectively impedes viral progression in the lungs. Deng et al. reported mRNA-encoded antibodies in a SARS-CoV-2

the control and treatment groups. H&E-stained sections (top row) and H&E-stained sections with blue highlights on the inflammatory area (bottom row) are shown. Scale bar, 1 mm. (E) The ratio of the inflammatory area to the total lung area was calculated. (F) Immunohistochemical staining of SARS-CoV-2 nucleocapsid for lung tissue. Scale bar, 50 μm. (G) The number of stained cells was counted and calculated as positive cells per square millimeter. Data are presented as means ± SEMs. *p* values were determined using the Kruskal-Wallis test, followed by Dunn's multiple comparisons test in comparison with the control group.

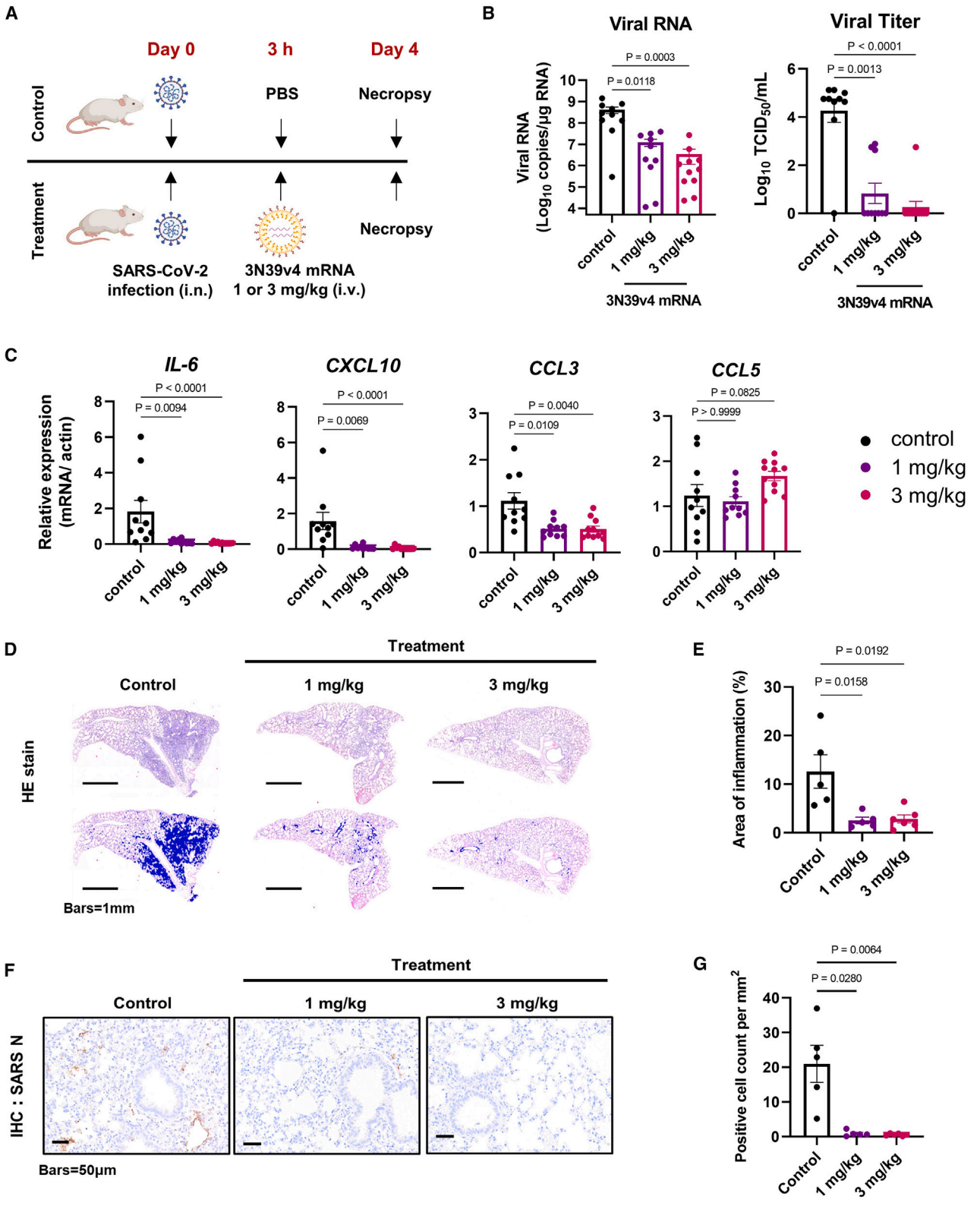

(legend on next page)

mouse-adapted strain, MASCp36, in which reduced viral propagation in the lungs following intravenous administration of LNP-formulated mRNA.[15] Deal et al. reported that LNP-formulated mRNA encoding IgA heavy, light, and J chains expressed dimeric pathogen-specific IgA localized to mucosal secretion and limited *Salmonella* Peyer's patch invasion in mice.[17] These reports further support the validated approach of using mRNA-based formulations for systemic effects. Under prophylactic conditions, 3N39v4 mRNA administered 1 day prior to viral inoculation demonstrated substantial efficacy. This could be partly attributed to the improved pharmacokinetic profile of 3N39v4 mRNA, resulting in a sustained high concentration of 3N39v4 for over 1 week. These data suggest the potential use of 3N39v4 mRNA as prophylaxis.

For respiratory infectious diseases, including SARS-CoV-2 infection, selective lung delivery of therapeutic agents is more beneficial than systemic administration because of its advantages, including rapid onset of action, sparing doses, higher concentrations delivered locally, and improved bioavailability. The majority of systemically administered LNPs target the liver; therefore, various strategies have been reported for engineering LNPs that target extrahepatic organs, including the lungs.[46] Several studies have demonstrated that the addition of cationic helper lipids to LNPs can improve lung delivery.[47,48] Tai et al. demonstrated that lung-selective delivery of the mRNA encoding a broadly neutralizing antibody more effectively protected female K18-hACE2 transgenic mice from challenge with the Beta or Omicron BA.1 variant compared to that with systemic LNP.[49] Moreover, inhalation of LNP is another strategy for targeted delivery to the lungs. Several reports have demonstrated the potential of inhalation-based mRNA therapies for lung diseases.[50–52] Additionally, we previously reported that inhaled aerosol administration of an engineered ACE2 decoy was effective at a 20-fold lower dose than the standard intravenous injection.[26] Considering that several inhalation-based LNP formulations have been tested in clinical trials,[46] engineering our LNP for selective delivery to the lungs could improve the benefits of our mRNA-encoded 3N39v4.

The successful translation of preclinical animal models to humans is crucial for drug development. Therefore, it is important to evaluate candidates from human-related samples and higher species.[53] We initially evaluated the LNP-formulated 3N39v4 mRNA expression in primary human hepatocytes. This revealed robust 3N39v4 production and confirmed its binding activity, which was comparable to that of recombinant 3N39v4. Next, we illustrated the elevated liver tropism of L202-based LNP in monkeys. Finally, in pharmacokinetic studies with monkeys at 1 mg/kg of 3N39v4 mRNA, a mean C_{max} of 5.5 μg/mL was observed with no apparent safety concerns. The 3N39v4-containing monkey plasma completely inhibited the authentic viral replication of subvariant XBB.1 and BA.2.75. Kim et al. reported a similar approach using LNP and mRNA-encoded human ACE2 decoy in mice.[54] However, their evaluation was limited to the expression in rodents, which contrasts with our study demonstrating robust therapeutic efficacy in SARS-CoV-2-infected mice and feasibility in monkeys. Therefore, we believe that the 3N39v4 mRNA has potential use in humans.

Despite the encouraging results, monkeys exhibited a 5-fold lower expression of 3N39v4 compared to that in mice at the same dose of 1 mg/kg (C_{max} 5.5 μg/mL in monkeys vs. 26.7 μg/mL in mice). Bahr-Mahmud et al. reported an LNP-formulated mRNA-encoded anti-Claudin 18.2 antibody and similarly observed that cynomolgus monkeys exhibited a 10-fold lower expression compared to rodents following a single intravenous administration.[22] Similarly, Maier et al. demonstrated the attenuated potency of LNP-formulated small interfering RNA (siRNA) in cynomolgus monkeys and discussed possible differences in the optimal formulations in mice and monkeys.[55] Recently, Lam et al. demonstrated a species-dependent optimized formulation, showing that (1) the particle size for monkeys (50–60 nm) was smaller than that for rodents (70–80 nm), and (2) the amount of PEG-lipid for monkeys (2–3% molar ratio in total lipids) was higher than that for rodents (1.5%–2%).[39] They eventually achieved an 8-fold increase in protein expression in monkeys compared with that in the original formulation.[39] In this study, the L202-based LNP exhibited conventional properties, with a size of approximately 70 nm and 1.5% PEG lipids. Although there is no description of the LNP formulation in the report by Bahr-Mahmud et al., this may explain the 5- to 10-fold lower expression in monkeys in our study and that of Bahr-Mahmud et al. Further LNP optimization may increase 3N39v4 expression in larger animals.

This study has several key limitations. First, protection against infection was demonstrated only in mice. Validation of drugs in one or more species can be valuable for assessing their potential utility. However, the 3N39v4 protein has been well investigated in various infection models, including hamsters[25] and monkeys.[26] Therefore, 3N39v4 mRNA is expected to work similarly. Second, the protection in mice was demonstrated under few experimental conditions. Considering the acute mouse model, the treatment schedule under

Figure 5. Therapeutic efficacy of 3N39v4 mRNA

(A) Experimental design. BALB/c mice were intranasally inoculated with mouse-adapted SARS-CoV-2 (MA10) at 1.0×10^4 $TCID_{50}$ (in 20 μL) at day 0. Then, mice were treated with either PBS (n = 10), 3N39v4 mRNA at 1 mg/kg (n = 10), or 3 mg/kg (n = 11) 3 h after and sacrificed at day 4. (B) Viral replication was measured in the lung. At the time of euthanasia, lung tissues were minced to measure viral RNA abundance (left) and viral titer (right) by qPCR analysis and $TCID_{50}$. (C) mRNA expression of IL-6, CXCL10, CCL3, and CCL5 in the lungs is shown for the control and treatment groups at day 4. (D) H&E staining for lung tissue sections of mice in the control and treatment groups. H&E-stained sections (top row) and H&E-stained sections with blue highlights on the inflammatory area (bottom row) are shown. Scale bar, 1 mm. (E) The ratio of the inflammatory area to the total lung area was calculated. (F) Immunohistochemical staining of SARS-CoV-2 nucleocapsid for lung tissue. Scale bar, 50 μm. (G) The number of stained cells was counted and calculated as positive cells per square millimeter. Data are presented as means ± SEMs. p values were determined using Kruskal-Wallis test, followed by Dunn's multiple comparisons test in comparison with control group.

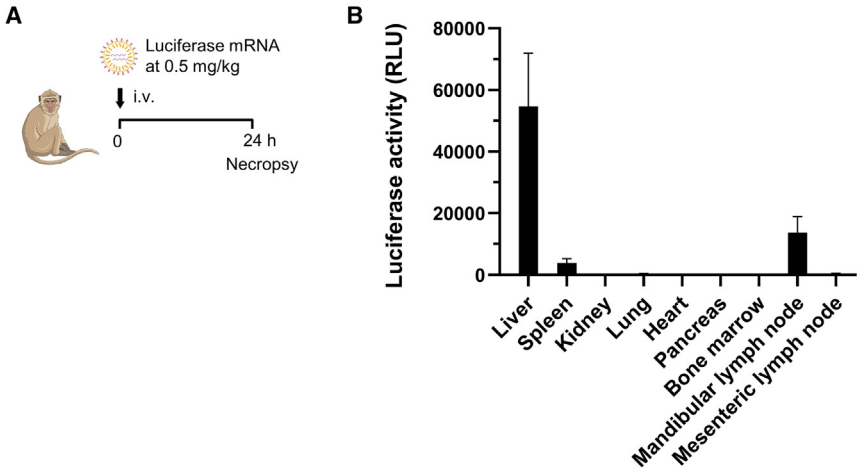

Figure 6. Biodistribution of LNP-mRNA in non-human primate

(A) Experimental design. Cynomolgus monkey (n = 3) received a single 60-min infusion of LNP-luciferase mRNA at 0.5 mg/kg. Organ samples (liver, spleen, lung, heart, kidney, pancreas, bone marrow, lymph node) were harvested 24 h post-dose and subject to luciferase expression assay. (B) Luciferase activity in each organ homogenate. Data are shown as means ± SEMs.

therapeutic conditions was set to mRNA administration 3 h after viral infection. In addition, the effective dose in mice was 1 mg/kg mRNA, which may be relatively high when considering its application in larger species. Further studies are required to determine their clinical use. Third, a small number of monkeys were tested for mRNA delivery. Despite clear evidence of liver delivery of L202-based LNP and 3N39v4 expression in monkeys, testing various conditions, including different or repeated doses, is beneficial for human translation. Biodistribution in the mandibular lymph nodes should also be tested for reproducibility, given that only a negligible signal was observed in the mesenteric lymph nodes. Nonetheless, we believe that these data provide solid justification for the application of 3N39v4 mRNA to the protection against SARS-CoV-2 variants.

MATERIALS AND METHODS

Study design

The SARS-CoV-2 infection experiment in mice was performed at biosafety level 3 facilities at the Research Institute for Microbial Diseases, Osaka University (Osaka, Japan). The study protocol was approved by the Institutional Committee of Laboratory Animal Experimentation at the Research Institute for Microbial Diseases. Other mouse experiments were approved by the Institutional Animal Care and Use Committee of Eisai Co. (Ibaraki, Japan), and were performed in accordance with the Animal Experimentation Regulations of Eisai Co. The animal care and experimental procedures were performed at an animal facility accredited by the Health Science Center for the Accreditation of Laboratory Animal Care and Use of the Japan Health Sciences Foundation. The biodistribution and pharmacokinetic studies in cynomolgus monkeys were conducted at Eisai and Shin Nippon Biomedical Laboratories (Kagoshima, Japan). The materials used in this study are summarized in Table S2.

mRNA production and LNP formulation

Codon-optimized mRNAs encoding ACE2 decoy (3N39v4) and firefly luciferase (Fluc) were prepared using T7 RNA polymerase-mediated *in vitro* transcription with a linearized DNA template. Each mRNA was initiated with a Cap1 structure, followed by a 5′ UTR, an open reading frame encoding the ACE2 decoy or Fluc, a 3′ UTR, and a polyadenylated tail of approximately 100 nt. Uridine was fully replaced with N1mΨ. After purification, the mRNA concentration was determined using UV light at 260 nm. mRNAs were cryopreserved at −70°C prior to use. The 3N39v4 mRNA was obtained from Elixirgen Scientific. Next, mRNAs were formulated with LNP using the ionizable lipid L202, with microfluidic mixing as previously reported.[35,56] The lipid composition consists of L202, distearoylphosphatidylcholine, cholesterol, and 1,2-dimyristoyl-*sn*-glycero-3-methoxypolyethylene glycol in an approximate molar ratio of 50/10/38.5/1.5. For the quality analysis of LNP-mRNA, the particle size, polydispersity index, and zeta potential (pH 7.5) were determined using dynamic light scattering with a Zetasizer Nano ZS (Malvern). Free and total mRNA concentrations in the LNPs were determined using a Quant-iT Ribogreen RNA assay kit (Invitrogen) and a fluorescence microplate reader (PerkinElmer). Encapsulation efficiency (EE, %) was calculated as follows: EE (%) = (1 − free siRNA concentration/total siRNA concentration) × 100. The pKa values of LNP-mRNA were measured based on the TNS fluorescent assay.[57]

3N39v4 expression in primary human hepatocytes

Cryopreserved primary human hepatocytes were purchased from Thermo Fisher Scientific. The cells were thawed and transferred to cryopreserved hepatocyte recovery medium (Thermo Fisher Scientific). After centrifugation at 100 × g for 10 min, the cell pellets were gently resuspended in Williams Medium E containing the CM3000 supplement (Thermo Fisher Scientific). Cells were seeded at a density of 6×10^4 cells/well in a 96-well plate coated with collagen I. After 6 h incubation, culture medium was changed to Williams Medium E containing CM4000 supplement (Thermo Fisher Scientific), human ApoE3 (final 1 μg/mL; Wako), and 3N39v4 mRNA/LNP (final 125, 250, and 500 ng/mL). After 48 h of incubation, the culture supernatant was collected, and 3N39v4 concentration was analyzed using ELISA.

Determination of 3N39v4 concentration by ELISA

The 3N39v4 concentrations in mouse plasma and monkey serum samples were determined using RBD ELISA. A Nunc-immuno MaxiSorp 96-well plate (Thermo Fisher Scientific) was coated with 2 μg/mL rabbit anti-6-His antibody (Bethyl Laboratories) at 4°C

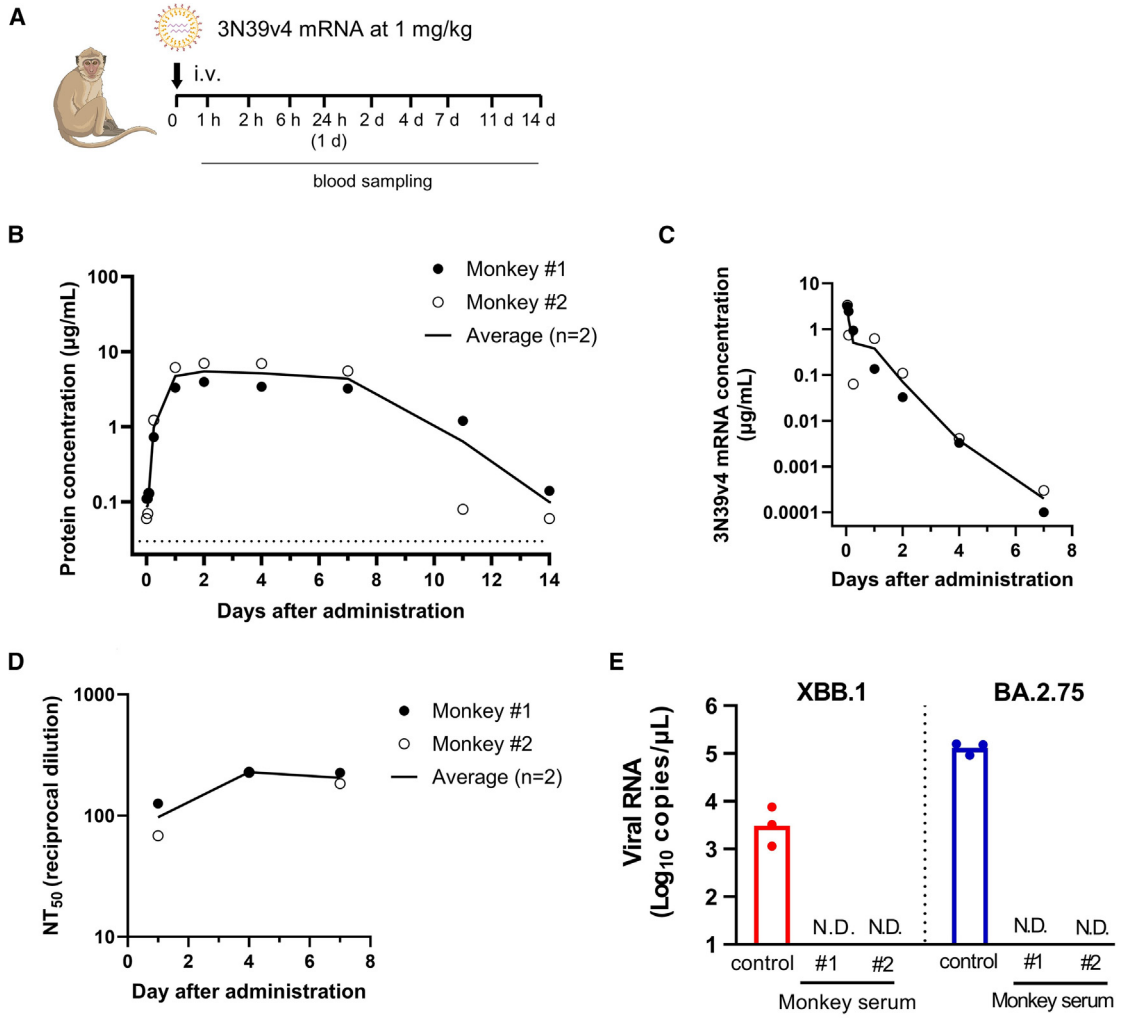

Figure 7. 3N39v4 mRNA in non-human primate

(A) Experimental design. Cynomolgus monkey (n = 2) received a single 60-min infusion of 3N39v4 mRNA at 1 mg/kg at day 0. Monkey serum was collected at 1 h, 2 h, 6 h, 24 h, 48 h, day 4, day 7, day 11, and day 14 post-dose. (B) We determined 3N39v4 expression using ELISA. (C) Pharmacokinetic profile of 3N39v4 mRNA in monkey sera determined by qPCR. Mean (n = 2) is shown with individual data points in closed and open circles. (D) Pseudoviral nebulization (D614G) using individual monkey sera at days 1, 4, and 7 post-dose. (E) Authentic viral neutralization (XBB.1 and BA.2.75) using pooled monkey sera of days 1, 4, and 7 post-dose (final 2-fold dilution). Data are presented as the mean of n = 3 technical replicates. N.D., not detected.

overnight. All subsequent steps were performed at 25°C, and the wells were washed with PBS-T (0.02% Tween 20) prior to each step. The wells were then blocked with 1% Block Ace (DS Pharma) and incubated with 2 nM RBD-His protein. Plasma and serum samples diluted in 1% Block Ace were added to the plate in duplicate and incubated. The 3N39v4 bound to RBD-His was detected using horseradish peroxidase (HRP)-conjugated goat anti-human IgG antibody (Bethyl Laboratories) with chromogen (3,3′,5,5′-tetramethylbenzidine, Seracare Life Sciences) as a substrate. After stopping the reaction with a stop solution (2N sulfuric acid, Wako), the absorbance was measured at 450 and 650 nm. The 3N39v4 concentration in the supernatant of primary human hepatocytes was determined using sandwich ELISA with secondary antibodies against human IgG as follows: the immunoplate was coated with 2 μg/mL goat anti-human IgG Fcγ fragment specific antibody (Jackson Immunoresearch), blocked with 1% Block Ace, and diluted samples were added. Detection with HRP-conjugated goat anti-human IgG antibody and the subsequent steps were the same as for the RBD ELISA. In both quantitative ELISAs, recombinant 3N39v4 protein was used as the standard, and calibration curves were fitted using a four-parameter logistic equation.

Binding affinity of 3N39v4 protein expressed *in vivo* or in primary human hepatocytes

To measure the RBD-binding affinity of 3N39v4 expressed by LNP-3N39v4 mRNA treatment, the concentration of 3N39v4 in mouse plasma or supernatant samples secreted from primary human

hepatocytes was determined using an anti-human IgG sandwich ELISA. The 4-fold serial dilutions of samples starting at 90 ng/mL were assayed using the RBD ELISA described above (differing only in that the concentration of RBD-His was 5 nM), and the dilution curves were regressed using the 4-PL logistic equation. In pharmacokinetic studies, each plasma sample (recombinant 3N39v4- or 3N39v4 mRNA-treated group) showing an equivalent 3N39v4 concentration was pooled (n = 5/group) and subjected to analysis.

SDS-PAGE and SEC analysis

To prepare 3N39v4 expressed by mRNA, Expi293F cells (Thermo Fisher Scientific) were maintained in Expi293 expression medium at 37°C and 8% CO_2. The cells were transiently transfected with 1 μg/10^6 cells/mL LNP-3N39v4 mRNA, and protein expression was induced for 4 days. The culture supernatant was harvested by centrifugation at 2,000 × g for 10 min at 25°C. rProtein A Sepharose Fast Flow resin (Cytiva) was added to the supernatant and gently stirred at 4°C for 1 h. The resin was subsequently loaded onto an Econo-Pac column (Bio-Rad) and washed with purification buffer (50 mM Tris-HCl, pH 8.0, and 200 mM NaCl). We eluted 3N39v4 with 0.1 M glycine-HCl (pH 3.9), and it was immediately neutralized by adding 1/20 vol of 1 M Tris-HCl (pH 8.0). The eluate was concentrated using an Amicon Ultra 50-kDa molecular weight cutoff (MWCO) (Merck Millipore) and subjected to SEC using a Superdex 200 Increase 10/300 column (Cytiva) pre-equilibrated with SEC buffer (50 mM HEPES-NaOH, pH 7.5, 200 mM NaCl). The peak fractions were concentrated with Amicon, flash-frozen in liquid nitrogen, and stored at −80°C.

The purified proteins were analyzed using SDS-PAGE with a 15% polyacrylamide gel (DRC) with and without 100 mM DTT and then stained with SimplyBlue SafeStain (Thermo Fisher Scientific).

To prepare the recombinant SARS-CoV-2 spike protein, a gene encoding residues 1–1,208 of the SARS-CoV-2 spike was synthesized and incorporated into the pcDNA3.4-TOPO vector (Thermo Fisher Scientific) with a GSAS substitution at the furin cleavage site (residues 682–685), D614G, and proline substitutions at residues 986 and 987 for stability,[58] followed by a C-terminal T4 fibritin trimerization motif, TEV protease cleavage site, FLAG tag, and a His9 tag. The resulting plasmid was used to transiently express spike proteins in Expi293F cells according to the manufacturer's protocol. The cell culture was collected 4 days after the transfection and incubated with Ni-nitrilotriacetic acid resin (Qiagen) for 1 h at 4°C with stirring. Bound proteins were washed with purification buffers containing 10 and 30 mM imidazole and then eluted with a purification buffer containing 350 mM imidazole. The eluted spike trimers were further purified using SEC with a Superose 6 Increase 10/300 column (Cytiva) pre-equilibrated with SEC buffer. The peak fractions were concentrated with Amicon Ultra 100-kDa MWCO, flash-frozen in liquid nitrogen, and stored at −80°C.

Cryo-EM data collection and image processing of 3N39v4

A droplet of 3 μL protein solution was applied to a glow-discharged Quantifoil R1.2/1.3 Au 300-mesh grid (Quantifoil Micro Tools). The grid was blotted for 5 s with a blot force of 15 and flash-frozen in liquid ethane using a Vitrobot Mark IV at 18°C and 100% humidity. Data were collected at 200 kV using a Talos Arctica electron microscope equipped with a Falcon 4 direct-electron detector. Images were acquired at a range of defocus from −1.0 to −2.5 μm, with a nominal magnification of 150,000, corresponding to a pixel size of 0.66 Å at the electron exposure of 9.34 $e^{-}Å^{-2}$/s and a total exposure time of 5.35 s, resulting in an accumulated exposure of 50 $e^{-}Å^{-2}$. Image processing was performed using RELION-5.[59] The movies were aligned and dose-weighted using the RELION implementation of MotionCor2.[60] The contrast transfer function parameters were estimated using CTFFIND4.1.[61] Template-based autopicked particles were extracted with a pixel size of 3.63 Å and subjected to multiple rounds of two-dimensional (2D) and 3D classifications.

3N39v4 expression in mice

For the pharmacokinetic study, male CD-1 mice (n = 5/group) received a single intravenous injection of either 5 mg/kg 3N39v4 protein or 1 mg/kg LNP-3N39v4 mRNA. Plasma samples were collected after 0.5, 2, 6, 24, 72, 168, and 240 h, and cryopreserved at −70°C prior to use. The plasma 3N39v4 concentrations were checked using ELISA. The pharmacokinetic parameters in individual animals were determined using model-independent analysis with Phoenix WinNonlin version 8.3 (Certara USA). For the dose-dependent activity and tolerability study, male CD-1 mice (n = 3/group) received a single intravenous administration of either saline- or LNP-formulated 3N39v4 mRNA (1, 3, or 10 mg/kg mRNA) on day 0. The mice were weighed on day 0 (prior to dosing), and on days 1 and 3 (prior to sacrifice). Plasma was collected at days 1 and 3, and cryopreserved at −70°C prior to use. The plasma 3N39v4 concentrations were checked using ELISA, and neutralization titer checked using pseudovirus and clinical chemistry. Blood biochemistry was measured using a Hitachi 7180 clinical analyzer.

SARS-CoV-2 neutralization assay using pseudovirus

Pseudotyped reporter virus assays were conducted as previously described.[31] With a plasmid encoding the BA.2.86 spike protein (Addgene catalog no. 208583) as a template, BA.2.86 and JN.1 with ΔC19 deletion (19 amino acids deleted from the C terminus) was cloned into pcDNA4TO (Invitrogen). Plasmids encoding other SARS-CoV-2 variants, Pangolin CoV GD-1, Bat CoV WIV1, and SARS-CoV-1 spike proteins, were developed previously.[4,26,31] Spike protein-expressing pseudoviruses with a luciferase reporter gene was prepared by transfecting plasmids (SpikeΔC19, psPAX2, and pLenti firefly) into LentiX-293T cells with Lipofectamine 3000 (Invitrogen). After 48 h, supernatants were harvested, filtered with a 0.45-μm low protein-binding filter (surfactant-free cellulose acetate), and frozen at −80°C. ACE-expressing 293T cells (293T/ACE2) were seeded at a density of 10,000 cells/well in 96-well plates. Pseudoviruses and a 3-fold dilution series of serum were incubated for 1 h, and this mixture was added to 293T/ACE2 cells. After preincubation for 1 h, the medium was changed. At 48 h post-infection, cellular expression of the luciferase reporter, indicative of viral infection, was determined using the ONE-Glo Luciferase Assay System (Promega).

Luminescence was measured using an Infinite F200 Pro System (Tecan). The assay for each serum sample was performed in triplicate, and the 50% neutralization titer was calculated using GraphPad Prism software.

Viruses

SARS-CoV-2 Omicron (BA.2.75: hCoV-19/Japan/TY41-716/2022, XBB1: hCoV-19/Japan/TY41-795/2022) strain was isolated at the National Institute of Infectious Diseases. These viruses were propagated in VeroE6/TMPRSS2 cells. Tissue cultures with a 50% infectious dose ($TCID_{50}$) of the viral stock were measured using VeroE6/TMPRSS2 cells. Mice-adapted-SARS-CoV-2 MA10[25] was generated using a circular polymerase extension reaction, as previously described.[62,63]

SARS-CoV-2 infection study in mice

The 10-week-old female BALB/c mice were purchased from SLC Japan or CLEA Japan. In the prophylactic model, the mice were pretreated with a single intravenous administration of either PBS or 3N39v4 mRNA at 1 or 3 mg/kg. After 24 h post-treatment, mice were anesthetized by isoflurane and challenged with MA10 (1.0×10^4 $TCID_{50}$ in 20 μL) via intranasal routes. After 4 days post-infection, the animals were euthanized, and the lungs were collected for qPCR analysis and virus titration. In the therapeutic model, mice were anesthetized with isoflurane and challenged with MA10 (1.0×10^4 $TCID_{50}$ in 20 μL) via the intranasal route. Three hours after infection, PBS or 3N39v4 mRNA at 1 or 3 mg/kg was administered intravenously. Four days post-infection, the animals were euthanized, and the lungs were collected for qPCR analysis and virus titration.

Histopathological analysis

The left lobe of each mouse was cut and processed to prepare formalin-fixed paraffin-embedded tissue samples. The samples were cut into 2-μm-thick tissue sections and stained with hematoxylin and eosin (H&E). The H&E-stained tissue sections were scanned using SLIDEVIEW VS200 (Olympus Life Science) to acquire whole-slide digital virtual slide images. Using the image analysis software QuPath, an algorithm was trained to classify the histological pattern of the inflammatory area, and the ratio of the inflammatory area to the total lung tissue area was calculated.

Immunohistochemistry

For immunohistochemistry, 2-μm-thick tissue sections were deparaffinized and heated at 121°C for 10 min in retrieval solution at pH 6.0 (Nichirei Bioscience). After washing with PBS, endogenous peroxidase was quenched with 3% hydrogen peroxide in PBS. Then, blocking was performed with 5% skim milk in PBS for 30 min, after which the tissue sections were incubated with in-house rabbit anti-SARS-CoV-2 N antibody[64] at 4°C overnight. The slides were washed with PBS and incubated with Histofine Simple Stain MAX PO (R) (Nichirei Bioscience, catalog no. 424141, RRID: AB_3073750) at room temperature for 40 min. After washing with PBS, positive signals were visualized using peroxidase-diaminobenzidine, and the sections were counterstained with H&E. The sections were scanned using SLIDEVIEW VS200 (Olympus Life Science) to acquire whole-slide digital virtual images. Positive cell densities were calculated using QuPath.

mRNA expression by qPCR analysis

For mRNA expression analysis in mouse lungs, total RNA was isolated from lung homogenates using ISOGENE II (NIPPON GENE). Real-time PCR was performed using a Power SYBR Green RNA-to-CT 1-Step Kit (Thermo Fisher Scientific) on a QuantStudio 3 real-time PCR system (Applied Biosystems). Relative quantitation of target mRNA levels was performed using the 2-ΔΔCT method. The values were normalized to those of the housekeeping gene β-actin. The following primers were used: β-actin, 5′-TTGCTGACAGGATGCAGAAG-3′ and 5'-GTACTTGCGCTCAGGAGGAG-3′; 2019-nCoV_N2, 5′- AAATTTTGGGGACCAGGAAC-3′ and 5′-TGGCAGCTGTGTAGGTCAAC-3′; IL-6, 5′-CCACTTCACAAGTCGGAGGCTTA-3′ and 5′-GCAAGTGCATCATCGTTGTTCATAC-3′; CCL3, 5′-AACCAGCAGCCTTTGCTCCC-3′ and 5′-GGTCTCTTTGGAGTCAGCGCA-3′; CCL5, 5′-AGATCTCTGCAGCTGCCCTCA-3′ and 5′-GGAGCACTTGCTGCTGGTGTAG-3′; CXCL10, 5′-GGCCATCAAGAATTTACTGAAAGCA-3′ and 5′-TCTGTGTGGTCCATCCTTGGAA-3′. The number of RNA copies in the culture medium was determined using qPCR analysis, as previously described.[31] Culture supernatants (5 μL) were mixed with 5 μL 2× RNA lysis buffer (2% Triton X-100, 50 mM KCl, 100 mM Tris-HCl pH 7.4, 40% glycerol, 0.4 U/μL of SUPERase·IN [Life Technologies]) and incubated at room temperature for 10 min, followed by the addition of 90 μL RNase free water. We added 2.5 μL volume of the diluted samples to 17.5 μL of a reaction mixture. Real-time PCR was performed using the Power SYBR Green RNA-to-CT 1-Step Kit (Applied Biosystems) and the QuantStudio 3 real-time PCR System (Applied Biosystems).

Neutralization assay using authentic virus

VeroE6/TMPRSS2 cells were seeded at 20,000 cells in 96-well plates and incubated overnight. The cells were then infected with SARS-CoV-2 (Omicron XBB.1 or BA.2.75) at an MOI of 0.1, together with an equivalent volume of pooled monkey sera. After 2 h, the cells were washed with fresh medium and incubated for 46 h with pooled monkey sera diluted 2-fold in fresh medium. The culture supernatants were collected and subjected to qPCR analysis.

Monkey study

For the biodistribution study, male cynomolgus monkeys (n = 3) received a single 60-min infusion (5 mL/kg/h) of LNP-formulated luciferase mRNA at 0.5 mg/kg mRNA. At 24 h after administration, the monkeys were euthanized to harvest a fraction of the tissues (liver, spleen, lung, heart, kidney, pancreas, bone marrow, and lymph nodes). The tissues were immediately placed in liquid nitrogen until frozen, then transferred to freezer at −70°C. For the luciferase assay, a fraction of the tissue was homogenized in Glo Lysis buffer (Promega). Normalized luminescence was measured using Steady-Glo (Promega) and bicinchoninic acid protein assay kit using a microplate

reader (PerkinElmer). For the pharmacokinetic study, male cynomolgus monkeys ($n = 2$) received a single 60-min infusion (5 mL/kg/h) of LNP-formulated 3N39v4 mRNA at 1 mg/kg mRNA on day 0. Serum samples were collected prior to dosing, and 1 h, 2 h, 6 h, 24 h, 48 h, 4 days, 7 days, 11 days, and 14 days after dosing; they were cryopreserved at −70°C prior to assay. The monkeys were weighed before dosing and on days 1, 2, 4, and 7.

Quantification of mRNA in monkey sera by qPCR

Monkey sera were mixed with spike-in control Fluc mRNA, and total mRNA was purified using an miRNeasy serum/plasma kit (Qiagen) following the manufacturer's instructions. Reverse transcription was performed with 2 μL total RNA using the PrimeScript RT kit (Takara). For qPCR analysis, each reaction mixture of a total of 10 μL contained 0.5 μL TaqMan probe for 3N39v4, 0.5 μL TaqMan probe for Fluc, 5.0 μL TaqMan Gene Expression Master Mix (Thermo Fisher Scientific), and 4 μL cDNA. qPCR analysis reactions were performed using a ViiA7 Real-Time PCR System (Applied Biosystems) at 95°C for 10 min, followed by 45 cycles of 95°C for 15 s and 60°C for 1 min. Custom-made TaqMan probes for 3N39v4 and Fluc were purchased from Thermo Fisher Scientific. Absolute quantification was performed using a standard curve constructed with a defined amount of target mRNA.

Statistical analysis

The Kruskal-Wallis test with Dunn's multiple comparisons for non-parametric data was used to analyze multiple comparisons. An unpaired two-tailed t test was used to analyze the pharmacokinetic parameters. GraphPad Prism (version 10.2.0, GraphPad Software) was used.

DATA AVAILABILITY

The data that support the findings of this study are available from the corresponding authors upon reasonable request.

ACKNOWLEDGMENTS

We thank Mr. Daisuke Takagi, Dr. Yumiko Tokusumi, and other members of Elixirgen Scientific for mRNA manufacturing; members of the cryo-EM facility at the High Energy Accelerator Research Organization (Japan) for the cryo-EM data collection; Dr. Hideaki Ogasawara (Eisai) for the mRNA quantification methodology; all members of Eisai and Sunplanet who kindly supported this work; and Nao Komatsu of WORLD INTEC for their help with the expression and purification of proteins. Figures were created using Bio-Render.com. This research was supported by AMED under grant nos. JP21fk010858 and JP22fk0108524. The cryo-EM research was supported by the Platform Project for Supporting Drug Discovery and Life Science Research (Basis for Supporting Innovative Drug Discovery and Life Science Research (BINDS)) from AMED under grant no. JP22ama121001.

AUTHOR CONTRIBUTIONS

Y.S. and Y.M. conceptualized the project. T.M., Y. Ida, T.S., Y. Itoh, S.N., K. Kondo, K. Kubara, K.N., H.M., R.W., and T.H. performed the experiments and analyzed the data. D.K., S.S., S.I., Y.U., Y.M., A.H., T.O., and J.M supervised the project. Y.S. wrote the original draft. Y.S., Y.M., A.H., and T.O. wrote, reviewed, and edited the manuscript.

DECLARATION OF INTERESTS

Some of the authors were employees of Eisai during the execution of this research project, as indicated in the affiliations.

SUPPLEMENTAL INFORMATION

Supplemental information can be found online at https://doi.org/10.1016/j.omtn.2025.102467.

REFERENCES

1. Li, G., Hilgenfeld, R., Whitley, R., and De Clercq, E. (2023). Therapeutic strategies for COVID-19: progress and lessons learned. Nat. Rev. Drug Discov. *22*, 449–475.
2. Webb, C., Ip, S., Bathula, N.V., Popova, P., Soriano, S.K.V., Ly, H.H., Eryilmaz, B., Nguyen Huu, V.A., Broadhead, R., Rabel, M., et al. (2022). Current Status and Future Perspectives on MRNA Drug Manufacturing. Mol. Pharm. *19*, 1047–1058.
3. Corbett, K.S., Edwards, D.K., Leist, S.R., Abiona, O.M., Boyoglu-Barnum, S., Gillespie, R.A., Himansu, S., Schäfer, A., Ziwawo, C.T., DiPiazza, A.T., et al. (2020). SARS-CoV-2 mRNA vaccine design enabled by prototype pathogen preparedness. Nature *586*, 567–571.
4. Alcantara, M.C., Higuchi, Y., Kirita, Y., Matoba, S., and Hoshino, A. (2023). Deep Mutational Scanning to Predict Escape from Bebtelovimab in SARS-CoV-2 Omicron Subvariants. Vaccines *11*, 711.
5. Kelley, B. (2020). Developing therapeutic monoclonal antibodies at pandemic pace. Nat. Biotechnol. *38*, 540–545.
6. von Delft, A., Hall, M.D., Kwong, A.D., Purcell, L.A., Saikatendu, K.S., Schmitz, U., Tallarico, J.A., and Lee, A.A. (2023). Accelerating antiviral drug discovery: lessons from COVID-19. Nat. Rev. Drug Discov. *22*, 585–603.
7. Chaudhary, N., Weissman, D., and Whitehead, K.A. (2021). mRNA vaccines for infectious diseases: principles, delivery and clinical translation. Nat. Rev. Drug Discov. *20*, 817–838.
8. Barbier, A.J., Jiang, A.Y., Zhang, P., Wooster, R., and Anderson, D.G. (2022). The clinical progress of mRNA vaccines and immunotherapies. Nat. Biotechnol. *40*, 840–854.
9. Rohner, E., Yang, R., Foo, K.S., Goedel, A., and Chien, K.R. (2022). Unlocking the promise of mRNA therapeutics. Nat. Biotechnol. *40*, 1586–1600.
10. Zhao, Y., Gan, L., Ke, D., Chen, Q., and Fu, Y. (2023). Mechanisms and research advances in mRNA antibody drug-mediated passive immunotherapy. J. Transl. Med. *21*, 693.
11. Pardi, N., Secreto, A.J., Shan, X., Debonera, F., Glover, J., Yi, Y., Muramatsu, H., Ni, H., Mui, B.L., Tam, Y.K., et al. (2017). Administration of nucleoside-modified mRNA encoding broadly neutralizing antibody protects humanized mice from HIV-1 challenge. Nat. Commun. *8*, 14630.
12. Narayanan, E., Falcone, S., Elbashir, S.M., Attarwala, H., Hassett, K., Seaman, M.S., Carfi, A., and Himansu, S. (2022). Rational Design and In Vivo Characterization of mRNA-Encoded Broadly Neutralizing Antibody Combinations against HIV-1 *11*, 67.
13. Chen, B., Chen, Y., Li, J., Wang, C., Song, W., Wen, Y., Lin, J., Wu, Y., and Ying, T. (2022). A Single Dose of Anti-HBsAg Antibody-Encoding mRNA-LNPs Suppressed HBsAg Expression: a Potential Cure of Chronic Hepatitis B Virus Infection. mBio *13*, e0161222.
14. Kose, N., Fox, J.M., Sapparapu, G., Bombardi, R., Tennekoon, R.N., de Silva, A.D., Elbashir, S.M., Theisen, M.A., Humphris-Narayanan, E., Ciaramella, G., et al. (2019). A lipid-encapsulated mRNA encoding a potently neutralizing human monoclonal antibody protects against chikungunya infection. Sci. Immunol. *4*, eaaw6647.
15. Deng, Y.Q., Zhang, N.N., Zhang, Y.F., Zhong, X., Xu, S., Qiu, H.Y., Wang, T.C., Zhao, H., Zhou, C., Zu, S.L., et al. (2022). Lipid nanoparticle-encapsulated mRNA antibody provides long-term protection against SARS-CoV-2 in mice and hamsters. Cell Res. *32*, 375–382.
16. Vanover, D., Zurla, C., Peck, H.E., Orr-Burks, N., Joo, J.Y., Murray, J., Holladay, N., Hobbs, R.A., Jung, Y., Chaves, L.C.S., et al. (2022). Nebulized mRNA-Encoded Antibodies Protect Hamsters from SARS-CoV-2 Infection. Adv. Sci. *9*, e2202771.
17. Deal, C.E., Richards, A.F., Yeung, T., Maron, M.J., Wang, Z., Lai, Y.T., Fritz, B.R., Himansu, S., Narayanan, E., Liu, D., et al. (2023). An mRNA-based platform for the delivery of pathogen-specific IgA into mucosal secretions. Cell Rep. Med. *4*, 101253.
18. Stadler, C.R., Bähr-Mahmud, H., Celik, L., Hebich, B., Roth, A.S., Roth, R.P., Karikó, K., Türeci, Ö., and Sahin, U. (2017). Elimination of large tumors in mice by mRNA-encoded bispecific antibodies. Nat. Med. *23*, 815–817.

19. Wang, Y., Tiruthani, K., Li, S., Hu, M., Zhong, G., Tang, Y., Roy, S., Zhang, L., Tan, J., Liao, C., and Liu, R. (2021). mRNA Delivery of a Bispecific Single-Domain Antibody to Polarize Tumor-Associated Macrophages and Synergize Immunotherapy against Liver Malignancies. Adv. Mater. *33*, e2007603.

20. Rybakova, Y., Kowalski, P.S., Huang, Y., Gonzalez, J.T., Heartlein, M.W., DeRosa, F., Delcassian, D., and Anderson, D.G. (2019). mRNA Delivery for Therapeutic Anti-HER2 Antibody Expression In Vivo. Mol. Ther. *27*, 1415–1423.

21. Wu, L., Wang, W., Tian, J., Qi, C., Cai, Z., Yan, W., Xuan, S., and Shang, A. (2022). Intravenous Delivery of RNA Encoding Anti-PD-1 Human Monoclonal Antibody for Treating Intestinal Cancer. J. Cancer *13*, 579–588.

22. Bahr-Mahmud, H., Ellinghaus, U., Stadler, C.R., Fischer, L., Lindemann, C., Chaturvedi, A., Diekmann, J., Woll, S., Biermann, I., Hebich, B., et al. (2023). Preclinical characterization of an mRNA-encoded anti-Claudin 18.2 antibody. OncoImmunology *12*, 2255041.

23. August, A., Attarwala, H.Z., Himansu, S., Kalidindi, S., Lu, S., Pajon, R., Han, S., Lecerf, J.M., Tomassini, J.E., Hard, M., et al. (2021). A phase 1 trial of lipid-encapsulated mRNA encoding a monoclonal antibody with neutralizing activity against Chikungunya virus. Nat. Med. *27*, 2224–2233.

24. Cox, M., Peacock, T.P., Harvey, W.T., Hughes, J., Wright, D.W., COVID-19 Genomics UK COG-UK Consortium, Willett, B.J., Thomson, E., Gupta, R.K., Peacock, S.J., and Robertson, D.L. (2023). SARS-CoV-2 variant evasion of monoclonal antibodies based on in vitro studies. Nat. Rev. Microbiol. *21*, 112–124.

25. Higuchi, Y., Suzuki, T., Arimori, T., Ikemura, N., Mihara, E., Kirita, Y., Ohgitani, E., Mazda, O., Motooka, D., Nakamura, S., et al. (2021). Engineered ACE2 receptor therapy overcomes mutational escape of SARS-CoV-2. Nat. Commun. *12*, 3802.

26. Urano, E., Itoh, Y., Suzuki, T., Sasaki, T., Kishikawa, J.I., Akamatsu, K., Higuchi, Y., Sakai, Y., Okamura, T., Mitoma, S., et al. (2023). An inhaled ACE2 decoy confers protection against SARS-CoV-2 infection in preclinical models. Sci. Transl. Med. *15*, eadi2623.

27. Kawase, W., Kurotaki, D., Suzuki, Y., Ishihara, H., Ban, T., Sato, G.R., Ichikawa, J., Yanai, H., Taniguchi, T., Tsukahara, K., and Tamura, T. (2021). Irf5 siRNA-loaded biodegradable lipid nanoparticles ameliorate concanavalin A-induced liver injury. Mol. Ther. Nucleic Acids *25*, 708–715.

28. Ishigooka, H., Katsumata, H., Saiga, K., Tokita, D., Motoi, S., Matsui, C., Suzuki, Y., Tomimatsu, A., Nakatani, T., Kuboi, Y., et al. (2022). Novel Complement C5 Small-interfering RNA Lipid Nanoparticle Prolongs Graft Survival in a Hypersensitized Rat Kidney Transplant Model. Transplantation *106*, 2338–2347.

29. Kuboi, Y., Suzuki, Y., Motoi, S., Matsui, C., Toritsuka, N., Nakatani, T., Tahara, K., Takahashi, Y., Ida, Y., Tomimatsu, A., et al. (2023). Identification of potent siRNA targeting complement C5 and its robust activity in pre-clinical models of myasthenia gravis and collagen-induced arthritis. Mol. Ther. Nucleic Acids *31*, 339–351.

30. Yamazaki, K., Kubara, K., Ishii, S., Kondo, K., Suzuki, Y., Miyazaki, T., Mitsuhashi, K., Ito, M., and Tsukahara, K. (2023). Lipid nanoparticle-targeted mRNA formulation as a treatment for ornithine-transcarbamylase deficiency model mice. Mol. Ther. Nucleic Acids *33*, 210–226.

31. Ikemura, N., Taminishi, S., Inaba, T., Arimori, T., Motooka, D., Katoh, K., Kirita, Y., Higuchi, Y., Li, S., Suzuki, T., et al. (2022). An engineered ACE2 decoy neutralizes the SARS-CoV-2 Omicron variant and confers protection against infection in vivo. Sci. Transl. Med. *14*, eabn7737.

32. Andries, O., Mc Cafferty, S., De Smedt, S.C., Weiss, R., Sanders, N.N., and Kitada, T. (2015). N(1)-methylpseudouridine-incorporated mRNA outperforms pseudouridine-incorporated mRNA by providing enhanced protein expression and reduced immunogenicity in mammalian cell lines and mice. J. Contr. Release *217*, 337–344.

33. Nance, K.D., and Meier, J.L. (2021). Modifications in an Emergency: The Role of N1-Methylpseudouridine in COVID-19 Vaccines. ACS Cent. Sci. *7*, 748–756.

34. Suzuki, Y., Miyazaki, T., Muto, H., Kubara, K., Mukai, Y., Watari, R., Sato, S., Kondo, K., Tsukumo, S.I., Yasutomo, K., et al. (2022). Design and lyophilization of lipid nanoparticles for mRNA vaccine and its robust immune response in mice and nonhuman primates. Mol. Ther. Nucleic Acids *30*, 226–240.

35. Kubara, K., Yamazaki, K., Miyazaki, T., Kondo, K., Kurotaki, D., Tamura, T., and Suzuki, Y. (2024). Lymph node macrophages drive innate immune responses to enhance the anti-tumor efficacy of mRNA vaccines. Mol. Ther. *32*, 704–721.

36. Di, J., Du, Z., Wu, K., Jin, S., Wang, X., Li, T., and Xu, Y. (2022). Biodistribution and Non-linear Gene Expression of mRNA LNPs Affected by Delivery Route and Particle Size. Pharm. Res. (N. Y.) *39*, 105–114.

37. Yamasoba, D., Kosugi, Y., Kimura, I., Fujita, S., Uriu, K., Ito, J., and Sato, K.; Genotype to Phenotype Japan G2P-Japan Consortium (2022). Neutralisation sensitivity of SARS-CoV-2 omicron subvariants to therapeutic monoclonal antibodies. Lancet Infect. Dis. *22*, 942–943.

38. Leist, S.R., Dinnon, K.H., 3rd, Schafer, A., Tse, L.V., Okuda, K., Hou, Y.J., West, A., Edwards, C.E., Sanders, W., Fritch, E.J., et al. (2020). A Mouse-Adapted SARS-CoV-2 Induces Acute Lung Injury and Mortality in Standard Laboratory Mice. Cell *183*, 1070–1085.e12.

39. Lam, K., Schreiner, P., Leung, A., Stainton, P., Reid, S., Yaworski, E., Lutwyche, P., and Heyes, J. (2023). Optimizing Lipid Nanoparticles for Delivery in Primates. Adv. Mater. *35*, e2211420.

40. Harris, C.T., and Cohen, S. (2024). Reducing Immunogenicity by Design: Approaches to Minimize Immunogenicity of Monoclonal Antibodies. BioDrugs *38*, 205–226.

41. Cunningham, O., Scott, M., Zhou, Z.S., and Finlay, W.J.J. (2021). Polyreactivity and polyspecificity in therapeutic antibody development: risk factors for failure in preclinical and clinical development campaigns. mAbs *13*, 1999195.

42. Beygmoradi, A., Homaei, A., Hemmati, R., and Fernandes, P. (2023). Recombinant protein expression: Challenges in production and folding related matters. Int. J. Biol. Macromol. *233*, 123407.

43. Tanaka, H., Hagiwara, S., Shirane, D., Yamakawa, T., Sato, Y., Matsumoto, C., Ishizaki, K., Hishinuma, M., Chida, K., Sasaki, K., et al. (2023). Ready-to-Use-Type Lyophilized Lipid Nanoparticle Formulation for the Postencapsulation of Messenger RNA. ACS Nano *17*, 2588–2601.

44. Zaman, R., Islam, R.A., Ibnat, N., Othman, I., Zaini, A., Lee, C.Y., and Chowdhury, E.H. (2019). Current strategies in extending half-lives of therapeutic proteins. J. Contr. Release *301*, 176–189.

45. Strohl, W.R. (2015). Fusion Proteins for Half-Life Extension of Biologics as a Strategy to Make Biobetters. BioDrugs *29*, 215–239.

46. Witten, J., Hu, Y., Langer, R., and Anderson, D.G. (2024). Recent advances in nanoparticulate RNA delivery systems. Proc. Natl. Acad. Sci. USA *121*, e2307798120.

47. Cheng, Q., Wei, T., Farbiak, L., Johnson, L.T., Dilliard, S.A., and Siegwart, D.J. (2020). Selective organ targeting (SORT) nanoparticles for tissue-specific mRNA delivery and CRISPR-Cas gene editing. Nat. Nanotechnol. *15*, 313–320.

48. LoPresti, S.T., Arral, M.L., Chaudhary, N., and Whitehead, K.A. (2022). The replacement of helper lipids with charged alternatives in lipid nanoparticles facilitates targeted mRNA delivery to the spleen and lungs. J. Contr. Release *345*, 819–831.

49. Tai, W., Yang, K., Liu, Y., Li, R., Feng, S., Chai, B., Zhuang, X., Qi, S., Shi, H., Liu, Z., et al. (2023). A lung-selective delivery of mRNA encoding broadly neutralizing antibody against SARS-CoV-2 infection. Nat. Commun. *14*, 8042.

50. Lokugamage, M.P., Vanover, D., Beyersdorf, J., Hatit, M.Z.C., Rotolo, L., Echeverri, E.S., Peck, H.E., Ni, H., Yoon, J.K., Kim, Y., et al. (2021). Optimization of lipid nanoparticles for the delivery of nebulized therapeutic mRNA to the lungs. Nat. Biomed. Eng. *5*, 1059–1068.

51. Li, B., Manan, R.S., Liang, S.Q., Gordon, A., Jiang, A., Varley, A., Gao, G., Langer, R., Xue, W., and Anderson, D. (2023). Combinatorial design of nanoparticles for pulmonary mRNA delivery and genome editing. Nat. Biotechnol. *41*, 1410–1415.

52. Kim, J., Jozic, A., Lin, Y., Eygeris, Y., Bloom, E., Tan, X., Acosta, C., MacDonald, K.D., Welsher, K.D., and Sahay, G. (2022). Engineering Lipid Nanoparticles for Enhanced Intracellular Delivery of mRNA through Inhalation. ACS Nano *16*, 14792–14806.

53. Loewa, A., Feng, J.J., and Hedtrich, S. (2023). Human disease models in drug development. Nat. Rev. Bioeng. *1*, 545–559. https://www.nature.com/articles/s44222-023-00063-3.

54. Kim, J., Jozic, A., Mukherjee, A., Nelson, D., Chiem, K., Khan, M.S.R., Torrelles, J.B., Martinez-Sobrido, L., and Sahay, G. (2022). Rapid Generation of Circulating and Mucosal Decoy Human ACE2 using mRNA Nanotherapeutics for the Potential Treatment of SARS-CoV-2. Adv. Sci. *9*, e2202556.

55. Maier, M.A., Jayaraman, M., Matsuda, S., Liu, J., Barros, S., Querbes, W., Tam, Y.K., Ansell, S.M., Kumar, V., Qin, J., et al. (2013). Biodegradable lipids enabling rapidly

eliminated lipid nanoparticles for systemic delivery of RNAi therapeutics. Mol. Ther. *21*, 1570–1578.

56. Sato, S., Sano, S., Muto, H., Kubara, K., Kondo, K., Miyazaki, T., Suzuki, Y., Uemoto, Y., and Ukai, K. (2024). Understanding the Manufacturing Process of Lipid Nanoparticles for mRNA Delivery Using Machine Learning. Chem. Pharm. Bull. *72*, 529–539.

57. Suzuki, Y., Hyodo, K., Tanaka, Y., and Ishihara, H. (2015). siRNA-lipid nanoparticles with long-term storage stability facilitate potent gene-silencing in vivo. J. Contr. Release *220*, 44–50.

58. Wrapp, D., Wang, N., Corbett, K.S., Goldsmith, J.A., Hsieh, C.L., Abiona, O., Graham, B.S., and McLellan, J.S. (2020). Cryo-EM structure of the 2019-nCoV spike in the prefusion conformation. Science *367*, 1260–1263.

59. Kimanius, D., Jamali, K., Wilkinson, M.E., Lövestam, S., Velazhahan, V., Nakane, T., and Scheres, S.H.W. (2024). Data-driven regularization lowers the size barrier of cryo-EM structure determination. Nat. Methods *21*, 1216–1221.

60. Zheng, S.Q., Palovcak, E., Armache, J.P., Verba, K.A., Cheng, Y., and Agard, D.A. (2017). MotionCor2: anisotropic correction of beam-induced motion for improved cryo-electron microscopy. Nat. Methods *14*, 331–332.

61. Rohou, A., and Grigorieff, N. (2015). CTFFIND4: Fast and accurate defocus estimation from electron micrographs. J. Struct. Biol. *192*, 216–221.

62. Miyamoto, Y., Itoh, Y., Suzuki, T., Tanaka, T., Sakai, Y., Koido, M., Hata, C., Wang, C.X., Otani, M., Moriishi, K., et al. (2022). SARS-CoV-2 ORF6 disrupts nucleocytoplasmic trafficking to advance viral replication. Commun. Biol. *5*, 483.

63. Torii, S., Ono, C., Suzuki, R., Morioka, Y., Anzai, I., Fauzyah, Y., Maeda, Y., Kamitani, W., Fukuhara, T., and Matsuura, Y. (2021). Establishment of a reverse genetics system for SARS-CoV-2 using circular polymerase extension reaction. Cell Rep. *35*, 109014.

64. Iwata-Yoshikawa, N., Shiwa, N., Sekizuka, T., Sano, K., Ainai, A., Hemmi, T., Kataoka, M., Kuroda, M., Hasegawa, H., Suzuki, T., and Nagata, N. (2022). A lethal mouse model for evaluating vaccine-associated enhanced respiratory disease during SARS-CoV-2 infection. Sci. Adv. *8*, eabh3827.